

A merger in the dusty, $z = 7.5$ galaxy A1689-zD1?

Kirsten K. Knudsen,^{1*} Darach Watson,² David Frayer,³ Lise Christensen,²
Anna Gallazzi,⁴ Michał J. Michałowski,⁵ Johan Richard⁶ and Jesús Zavala^{2,7}

¹Department of Earth and Space Sciences, Chalmers University of Technology, Onsala Space Observatory, SE-43992 Onsala, Sweden

²Dark Cosmology Centre, Niels Bohr Institute, University of Copenhagen, Juliane Maries Vej 30, DK-2100 Copenhagen Ø, Denmark

³National Radio Astronomy Observatory, PO Box 2, Green Bank, WV 24944, USA

⁴INAF-Osservatorio Astrofisico di Arcetri, Largo Enrico Fermi 5, I-50125 Firenze, Italy

⁵SUPA (Scottish Universities Physics Alliance), Institute for Astronomy, University of Edinburgh, Royal Observatory, Blackford Hill, Edinburgh EH9 3HJ, UK

⁶Univ Lyon, Univ Lyon1, Ens de Lyon, CNRS, Centre de Recherche Astrophysique de Lyon UMR5574, F-69230 Saint-Genis-Laval, France

⁷Center for Astrophysics and Cosmology, Science Institute, University of Iceland, Dunhagi 5, 107 Reykjavik, Iceland

Accepted 2016 November 23. Received 2016 November 21; in original form 2016 March 9

ABSTRACT

The gravitationally lensed galaxy A1689-zD1 is one of the most distant spectroscopically confirmed sources ($z = 7.5$). It is the earliest known galaxy where the interstellar medium (ISM) has been detected; dust emission was detected with the Atacama Large Millimetre Array (ALMA). A1689-zD1 is also unusual among high-redshift dust emitters as it is a sub- L^* galaxy and is therefore a good prospect for the detection of gaseous ISM in a more typical galaxy at this redshift. We observed A1689-zD1 with ALMA in bands 6 and 7 and with the Green Bank Telescope (GBT) in band Q . To study the structure of A1689-zD1, we map the mm-thermal dust emission and find two spatial components with sizes about 0.4 – 1.7 kpc (lensing-corrected). The rough spatial morphology is similar to what is observed in the near-infrared with *HST* and points to a perturbed dynamical state, perhaps indicative of a major merger or a disc in early formation. The ALMA photometry is used to constrain the far-infrared spectral energy distribution, yielding a dust temperature ($T_{\text{dust}} \sim 35\text{--}45$ K for $\beta = 1.5 - 2$). We do not detect the CO(3-2) line in the GBT data with a 95 per cent upper limit of 0.3 mJy observed. We find a slight excess emission in ALMA band 6 at 220.9 GHz. If this excess is real, it is likely due to emission from the [C II] 158.8 μm line at $z_{[\text{C II}]} = 7.603$. The stringent upper limits on the [C II] L_{FIR} luminosity ratio suggest a [C II] deficit similar to several bright quasars and massive starbursts.

Key words: galaxies: evolution – galaxies: formation – galaxies: high-redshift – galaxies: ISM – submillimetre: galaxies.

1 INTRODUCTION

With the increasing number of galaxies with spectroscopically confirmed redshifts $z > 7$ (Vanzella et al. 2011; Ono et al. 2012; Schenker et al. 2012; Shibuya et al. 2012; Finkelstein et al. 2013; Oesch et al. 2015; Watson et al. 2015; Zitrin et al. 2015; Oesch et al. 2016; Song et al. 2016), the possibilities for quantifying and understanding the processes that take place during the earlier stages of galaxy formation and evolution improve significantly. Spectroscopic redshifts are necessary not only for determining the distance, but also for enabling detailed follow-up observations. For the $z > 6$ range, multiwavelength studies of quasars and submillimetre galaxies have been very successful (e.g. Maiolino et al. 2005;

Venemans et al. 2012; Riechers et al. 2013; Wang et al. 2013; Bañados et al. 2015; Cicone et al. 2015; Willott, Bergeron & Omont 2015a; Venemans et al. 2016), however those sources represent the very bright end of the luminosity function, and they are not representative of the overall galaxy population.

Recent searches for dust and far-infrared emission lines towards $z \sim 7$ galaxies have resulted in only a few line detections (e.g. Kanekar et al. 2013; Ouchi et al. 2013; González-López et al. 2014; Ota et al. 2014; Maiolino et al. 2015; Schaerer et al. 2015; Willott et al. 2015b; Bradač et al. 2016; Knudsen et al. 2016; Pentericci et al. 2016). These galaxies have non-detections or marginal detections in the far-infrared continuum suggesting that the dust mass is relatively low. However, Watson et al. (2015) found a clear detection of dust emission towards the spectroscopically confirmed $z = 7.5$ galaxy Abell 1689-zD1 (A1689-zD1; Bradley et al. 2008) with an estimated dust mass comparable to that of the Milky Way.

* E-mail: kirsten.knudsen@chalmers.se

Table 1. Summary of the ALMA observations, project 2013.1.01064.S. Columns are: ALMA band number, date of observations, number of antennas (N_{ant}), two columns of calibrators used for each set of observations, and the central frequency of each spectral window except for the continuum observations where we give the central frequency of the continuum band.

	Date (DD-MM-YYYY)	N_{ant}	Flux	Calibrators Bandpass + Gain	$\nu_{\text{spw, central}}$ (GHz)
Band 6	08-12-2014	35	Ganymede	J1256–0547	217.455, 219.036, 220.456
	08-12-2014	35	Ganymede	J1256–0547	222.306, 223.806, 225.306
	08-12-2014	35	Titan	J1256–0547	227.156, 228.606, 230.156
Band 7	05-05-2015	34	J1256–0547	J1256–0547	343.5 (continuum)
	11-04-2016	42	J1256–0547	J1256–0547	343.5 (continuum)

A1689-zD1 is strongly lensed by a factor of 9.3, thus providing constraints on a sub- L^* galaxy (sub- L^* for $z \sim 7.5$). The estimated stellar mass is $\sim 1.7 \times 10^9 M_{\odot}$ and a total star formation rate (SFR) of $\sim 12 M_{\odot} \text{ yr}^{-1}$, which is dominated by dust-obscured star formation (Watson et al. 2015). Given the relatively short time after the big bang, it is unclear what mechanisms have produced such a large dust mass in this galaxy (e.g. Michałowski 2015).

In this paper, we present a follow-up study of A1689-zD1 aimed at a detailed investigation of the structure of the dust emission and thus the distribution of obscured star formation. Furthermore, we report observations of emission lines from [C II] 1900.537 GHz and CO(3-2) in order to study the properties of the interstellar medium (ISM) and accurately measure the systemic redshift. In Section 2, we present Atacama Large Millimetre Array (ALMA) and Green Bank Telescope (GBT) observations. In Section 3, we show the results of the observations and place it in the context of previous observations. We discuss the implications of the results in Section 4. Throughout the paper we assume a Λ CDM cosmology with $H_0 = 67.3 \text{ km s}^{-1} \text{ Mpc}^{-1}$, $\Omega_M = 0.315$, and $\Omega_{\Lambda} = 0.685$ (Planck Collaboration XVI 2014).

2 OBSERVATIONS

2.1 ALMA observations

A1689-zD1 was observed with ALMA during Cycle-2 with the observations carried out during 2014 December using band 6, and 2015 May and 2016 April with band 7. The purpose of the band-6 observations was to search for the redshifted [C II] line and, as the optical redshift is determined from the Lyman- α break and not from emission lines (Watson et al. 2015), we designed the observations to cover a large-frequency range. The receiver was tuned with three different setups, each with three spectral windows in one side band, which enabled continuous coverage from 216.51 to 231.06 GHz corresponding to the redshift range $z = 7.225 - 7.778$ for [C II].¹ The band 7 receiver was tuned to 343.5 GHz for continuum measurements. The telescope configuration has baselines extending between 15 and 348 m. Table 1 summarizes the details of the observations including a list of the calibrators.

CASA (COMMON ASTRONOMY SOFTWARE APPLICATION;² McMullin et al. 2007) was used for reduction, calibration, and imaging. The

results from the pipeline reduction³ carried out by the observatory was generally sufficient with only some minor extra flagging, which did not change the final result. The exception to this was the flux calibration of the final band-7 observations, for which the flux calibration had to be adjusted with updated flux density values for the calibrator J1256–0547 (a.k.a. 3C279). This update corresponded to about 10 per cent. We note that according to the ALMA calibrator source catalogue,⁴ 3C279 was variable up to 30 per cent in the month before our observations in 2016, though in 2016 April it appears to have been more stable. While individual fluxes for 3C279 have ~ 5 per cent errors, we place a conservative flux calibration uncertainty of 10 per cent for our band-6 results. Continuum maps were made for both the band-6 and band-7 data. Using natural weighting, the obtained rms is $21 \mu\text{Jy beam}^{-1}$ and $45 \mu\text{Jy beam}^{-1}$, respectively. Additionally, a spectral cube was created for the band-6 data, and with natural weighting in channels of 26 km s^{-1} width, the rms is $\sim 0.5 - 0.8 \text{ mJy beam}^{-1} \text{ channel}^{-1}$ (typically the highest noise is towards the highest frequency across the spectrum).

Similar to our description in Watson et al. (2015), the most conservative estimate of the astrometric uncertainty is half the beam dimensions, meaning $\sim 0.65 \text{ arcsec} \times 0.34 \text{ arcsec}$. There is no notable emission detected from the nearby, low- z galaxy seen 1.5 arcsec from A1689-zD1.

We report the serendipitous detection of a background source in the band-6 data in a forthcoming paper (Knudsen et al., in preparation).

2.2 GBT observations

The GBT was used to search for the redshifted CO(3-2) line ($\nu_{\text{rest}} = 345.796 \text{ GHz}$). The dual-beam Q -band receiver was tuned to a central frequency of 40.265 GHz covering the frequency range of 38.71–42.65 GHz, which corresponds to $z_{\text{CO(3-2)}} = 7.11 - 7.93$. Five observing sessions were carried out between 2014-09-18 and 2014-10-30. Observing scans were taken with the ‘SubBeamNod’ mode which used the subreflector to switch between the two beams every 6 s. We observed the bright nearby quasar 3C279 every 50–60 min to point and focus the telescope and to monitor the gain of the system.

We used the new GBT spectrometer VEGAS for the spectral-line observations. Four overlapping spectrometers (VEGAS mode-1) were used to cover the bandwidth for each beam and for both circular polarizations with a raw channel resolution of 1.465 MHz. GBTIDL was used to carry out the data reduction and calibration.

¹ This frequency range was selected based on the original error range to a simple fit to the Lyman- α break in the X-Shooter spectrum. However, a more conservative estimate of the uncertainty based on multiple methods gives a somewhat larger range and is quoted in Watson et al. (2015).

² <https://casa.nrao.edu>

³ For details on the pipeline, see <https://almascience.eso.org/documents-and-tools/>

⁴ almascience.eso.org/sc/

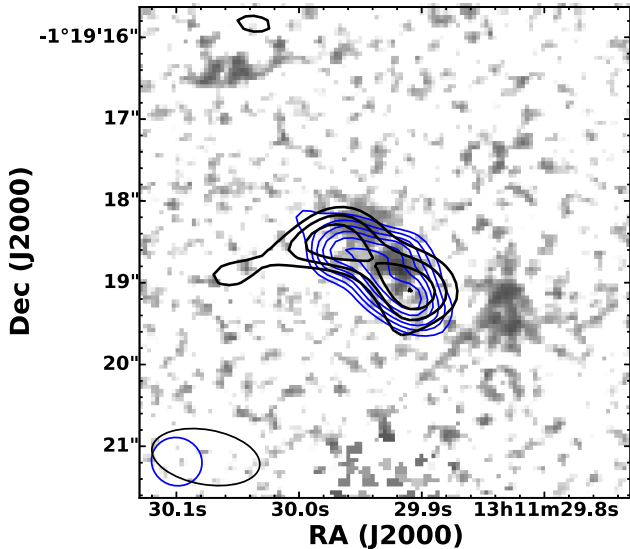


Figure 1. *HST* WFC3 F160W image overlaid with the contours of the ALMA band-6 and -7 observations. The ALMA band-6 continuum, shown in black, imaged with a Briggs robust parameter of 0 resulting in an image resolution of $1.33 \text{ arcsec} \times 0.67 \text{ arcsec}$ (PA = 80°), which results in an rms of $\sigma = 30 \text{ } \mu\text{Jy}$. The contours are in steps of 90, 120, 150, and 180 μJy . The blue contours show the band-7 observations, imaged using natural weighting (resulting beam size of $0.62 \text{ arcsec} \times 0.58 \text{ arcsec}$, PA = 67°) and with an rms of $\sigma = 45 \text{ } \mu\text{Jy}$; contours are 3σ , 4σ , 5σ , 6σ , 7σ , and 8σ .

The data have been corrected for the atmosphere and losses due to drifts in pointing and focus during the observations. Observations of 3C286 were used to derive the absolute calibration scale of the data. The uncertainty on the flux scale for the data is estimated to be 15 per cent. For a channel resolution of 1.465 MHz, we achieved 1σ rms of 0.267 mJy, and smoothed to 8.79 MHz (6 channels) the measured rms is 0.14 mJy; 8.79 MHz corresponds to 65 km s^{-1} for $\nu = 40.6 \text{ GHz}$.

3 RESULTS

3.1 Continuum

A1689-zD1 is detected in both bands 6 and 7 in continuum at $>10\sigma$. The emission is resolved with the structure showing two components. In Fig. 1, we show the bands 6 and 7 contours overlaid on an *Hubble Space Telescope* (*HST*) near-infrared image. Using the program *UVMULTIFIT* (Marti-Vidal et al. 2014) assuming a circular 2D Gaussian, we fit both bands together and measure a diameter (FWHM) of $0.52 \pm 0.12 \text{ arcsec}$ and $0.62 \pm 0.12 \text{ arcsec}$ for the two components (NE and SW, respectively); in the fit we have allowed for an astrometric offset between the two bands and find an insignificant offset in right ascension of $0.008 \pm 0.108 \text{ arcsec}$, while in declination the offset is $0.166 \pm 0.065 \text{ arcsec}$. Within the uncertainties, the two components have the same size. We note that fitting an elliptical 2D Gaussian function does not improve the results and the estimated major–minor axis ratio is consistent with one within the estimated uncertainties. Lensing magnification⁵ is

⁵ The estimates of the lensing magnification are based on an updated mass model of Abell 1689 (Limousin et al. 2007; Richard et al., in preparation) with the calculations done using *LENSTOOL* (Jullo et al. 2007; Jullo & Kneib 2009).

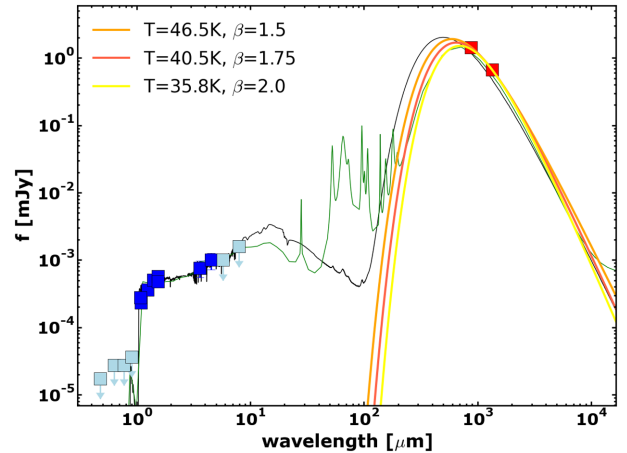


Figure 2. The optical-to-mm SED of A1689-zD1. The optical and infrared measurements come from Watson et al. (2015) and Bradley et al. (2008). The red, orange, and yellow lines show a modified blackbody for the best-fitting temperature for varying β -values. The ALMA photometry has been corrected for the CMB effect according to the $\beta = 1.75$ and $T = 40.5 \text{ K}$. The black and green lines show the best-fitting SED models using *MAGPHYS* and *GRASIL*.

estimated to be 1.5×6.5 with the axis of the largest magnification roughly along a position angle 90° , which implies that the smallest scale in that direction is about 0.4 kpc. This could indicate that the two clumps are somewhat elongated (0.41–0.49 kpc by 1.8–2.1 kpc with an uncertainty of about 50 per cent) as also seen in the lensing reconstruction of Bradley et al. (2008), however, the ALMA data does not have sufficient quality to further reaffirm this. The estimated area for both clumps together is $\sim 1 \text{ kpc}^2$, consistent with the estimate based on the *HST* near-infrared data (Watson et al. 2015).

From the *UVMULTIFIT* results we also obtain an estimate of the flux density of $f_{B7} = 1.33 \pm 0.14 \text{ mJy}$ (the sum of 0.58 ± 0.09 and $0.75 \pm 0.11 \text{ mJy}$, for NE and SW, respectively) and $f_{B6} = 0.56 \pm 0.1 \text{ mJy}$ (sum of 0.20 ± 0.08 and $0.36 \pm 0.06 \text{ mJy}$ for NE and SW, respectively). The errors reflect the uncertainties of the flux estimate and the errors on the total flux density are obtained from adding the individual errors in quadrature.

We use the photometric data points to constrain the far-infrared spectral energy distribution (SED). The observed frequencies correspond to rest-frame wavelengths of 157.6 μm and 102.7 μm , respectively, for $z = 7.5$. This means we are probing close to the peak of the dust emission. In Fig. 2, we show the measured fluxes together with the rest of the SED as presented in Watson et al. (2015). We constrain the temperature of a modified blackbody spectrum using the ratio of the fluxes from bands 7 and 6, where the modified blackbody function is described as $\nu^\beta B_\nu(T)$. For $z = 7.5$, the cosmic microwave background (CMB) temperature is $\sim 23.4 \text{ K}$. We estimate that the CMB would increase the temperature by ~ 1 per cent and that $\sim 5 - 23$ per cent of the intrinsic flux is missed due to the CMB radiation depending on the dust temperature, following the analysis of da Cunha et al. (2013). When estimating the dust temperature of A1689-zD1, we take the missed flux into account, but ignore the small change in temperature. In Fig. 3, we show how an estimated flux ratio changes with temperature for three different β -values and compare this to our measured flux ratio of $f_{\text{band-7}}/f_{\text{band-6}} \sim 2.4$. We find the best-fitting values of $T \sim 46.5, 40.5, \text{ and } 35.8 \text{ K}$ for $\beta = 1.5, 1.75, \text{ and } 2.0$, respectively. When not taking into account the effects of the CMB, the temperature estimates would be

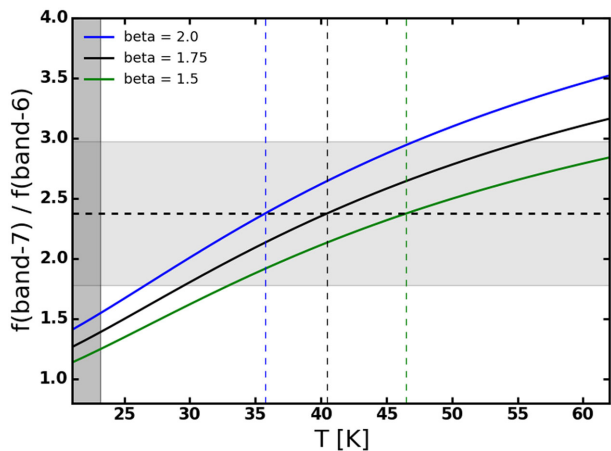


Figure 3. The estimated flux ratio for the band 6 to band 7 ratio as a function of temperature for a modified blackbody spectrum including corrections for the CMB radiation field; the errors on the two-flux estimates include both the uncertainty from the flux density estimate as well as a 10 per cent uncertainty on the absolute flux calibration. The horizontal dashed line shows the measured ratio with the grey shaded area indicating the error. The vertical grey shaded area towards low temperature indicates the $z = 7.5$ CMB temperature.

about 5 K higher. For $T = 40.5$ K and $\beta = 1.75$, the far-infrared luminosity is $1.7 \times 10^{12} L_{\odot}$ ($1.8 \times 10^{11} L_{\odot}$ after correcting for magnification); we note that the fraction of missed flux is ~ 8 and ~ 16 per cent for bands 7 and 6, respectively. Using the two other estimates for $\beta = 1.5$ and 2.0, the luminosity would increase/decrease by about 20 per cent. Given the uncertainties, this is in agreement with the estimate and assumptions made in Watson et al. (2015).

We update the MAGPHYS (da Cunha, Charlot & Elbaz 2008) and GRASIL (Silva et al. 1998; Iglesias-Páramo et al. 2007; Michałowski, Hjorth & Watson 2010) SED model fits from Watson et al. (2015) using the new ALMA band 6 + 7 photometry including the same correction for CMB effects as described in the previous paragraph. We find the derived parameters to be: $\text{SFR} = 12_{-3}^{+4} M_{\odot} \text{ yr}^{-1}$, $\log(M_{\text{stellar}}/M_{\odot}) = 9.3_{-0.14}^{+0.13}$, and $\log(M_{\text{dust}}/M_{\odot}) = 7.6_{-0.18}^{+0.27}$ from MAGPHYS, and $\text{SFR} = 14 \pm 8 M_{\odot} \text{ yr}^{-1}$, $\log(M_{\text{stellar}}/M_{\odot}) = 9.4 \pm 0.1$, and $\log(M_{\text{dust}}/M_{\odot}) = 7.2 \pm 0.2$ from GRASIL. The new and

deeper ALMA measurements, provide a better constraint on the far-infrared SED, e.g. for the dust temperature. The largest change in the derived parameters compared to Watson et al. (2015) is the lower nominal dust mass from the GRASIL fit, though this is consistent within the uncertainties. We plot the updated SED models in Fig. 2 and note that while the models are quite similar, the largest difference is found on the Wien’s tail and mid-infrared range. That is a wavelength range which is difficult to cover with present instrumentation, however, part of it can be studied soon with the James Webb Space Telescope.

3.2 [C II] line search

We extract the spectrum from the band-6 data at the position of A1689-zD1 to search for the [C II] 1900.537 GHz line, shown in Fig. 4 (note that the spectrum shown in the figure is Hanning smoothed and the rms is ~ 0.3 mJy). The redshift range that the spectrum covers corresponds to $z_{[\text{C II}]} = 7.2253 - 7.778$. No strong emission line is detected. We investigate all tentative emission features above 0.6 mJy (corresponding to 2σ ; indicated in Fig. 4) and create maps integrated over 100 MHz; the images are shown in Appendix A. At $\nu = 220.903$ GHz we find a 3σ detection, which in spatial distribution also would correspond to the position of A1689-zD1. The features at $\nu = 220.339$, 223.77, and 228.0 GHz also show 3σ sources in the imaging, however, with a lower spatial overlap. If the spectral feature at 220.903 GHz is indeed a weak detection of the [C II] line, fitting a Gaussian function implies a peak flux density of $S_{\text{peak}} = 0.77 \pm 0.20$ mJy beam $^{-1}$, FWHM line width of $\Delta V = 163 \pm 49$ km s $^{-1}$, and a velocity integrated intensity $I_{[\text{C II}]} = 0.126 \pm 0.050$ Jy km s $^{-1}$ (the error on the velocity integrated intensity is derived from regular error propagation of the Gaussian fit), and a redshift of $z_{[\text{C II}]} = 7.6031 \pm 0.0004$. We show the tentative line and the image of the integrated line in Fig. 5. Under the assumption that this is indeed a detection of [C II], this would correspond to a line luminosity of $L_{[\text{C II}]} \sim 1.7 \times 10^8 L_{\odot}$ ($1.8 \times 10^7 L_{\odot}$ after correcting for the lensing magnification of $\mu = 9.3$) using $L_{[\text{C II}]} = 1.04 \times 10^{-3} S \Delta V D_L^2 \nu_{\text{obs}}$, where $S \Delta V$ is the velocity integrated flux density, D_L is the luminosity distance, and ν_{obs} is the observer-frame frequency (e.g. Solomon & Vanden Bout 2005; Carilli & Walter 2013). Given that this is only a possible detection, we use the line luminosity as an upper limit.

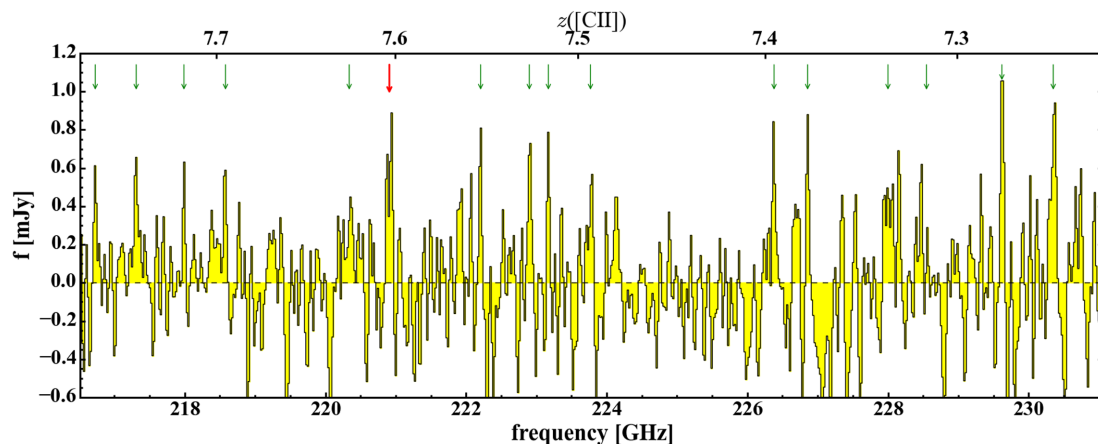


Figure 4. The ALMA band-6 spectrum extracted at the position of the dust continuum source. The spectrum is binned to 26 km s^{-1} per channel, Hanning smoothed by three channels, the continuum has been subtracted, and the whole covered frequency range is shown. The range corresponds to $z_{[\text{C II}]} = 7.2253 - 7.778$. The red arrow indicates the frequency of the tentative detection, see Fig. 5, and the green arrows indicate the frequencies investigated in the search for the [C II] line; images are shown in Appendix A.

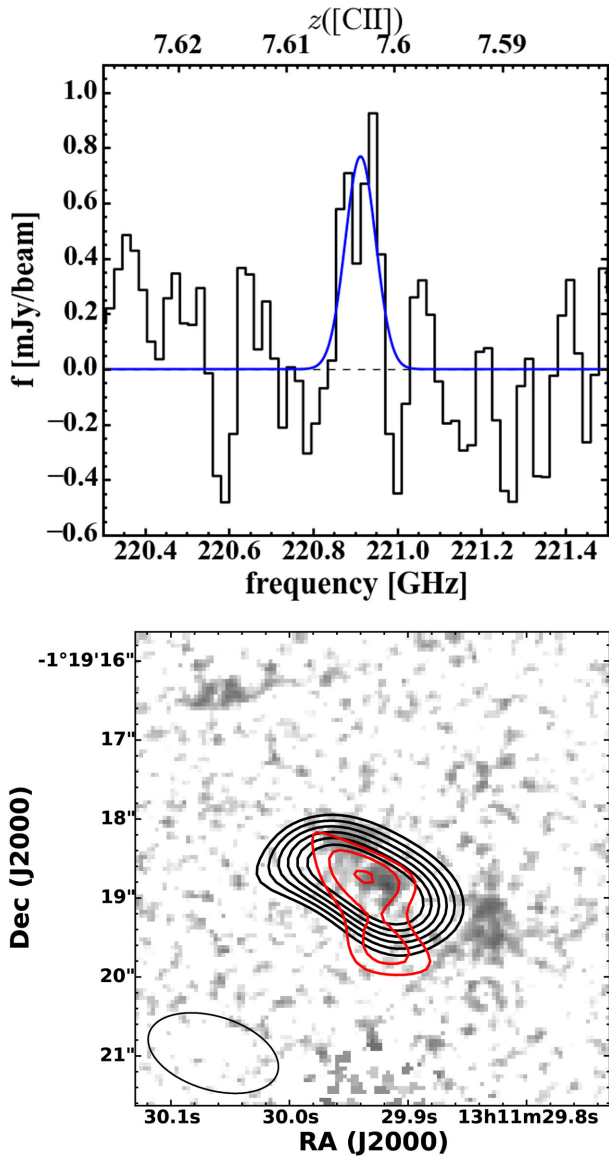


Figure 5. Upper panel: ALMA spectrum from Fig. 4, zoomed to the tentative detection at $\nu = 220.91$ GHz. The blue line shows the Gaussian fit to the line, which yields a peak flux density of $S_{\text{peak}} = 0.77 \pm 0.20$ mJy beam $^{-1}$ and an integrated line intensity of $I_{[\text{C II}]}$ = 0.126 ± 0.050 Jy km s $^{-1}$. Lower panel: the integrated image is shown as red contours (2σ , 2.5σ , and 3σ) overlaid on the near-infrared image (see Fig. 1) with the black contours showing the continuum imaged with natural weighting (5σ , 6σ , 7σ , 8σ , 9σ , 10σ); the natural weighting produces an image with lower resolution than e.g. is presented in Fig. 1. We note that the faint near-infrared source eastwards of the ALMA contours is a low-redshift galaxy (Watson et al. 2015).

3.3 CO(3-2) line search

In the GBT spectrum we do not detect the CO(3-2) line; the spectrum is shown in Fig. 6. The redshift range covered by the spectrum is $z_{\text{CO}32} = 7.12 - 7.93$. We place a 3σ limit for the same line width as the tentative [C II] line. This corresponds to $L'_{\text{CO}32} = 8.6 \times 10^9$ K km s $^{-1}$ pc 2 (9.0×10^8 K km s $^{-1}$ pc 2 after correcting for lensing) and $L_{\text{CO}32} = 1.1 \times 10^7 L_{\odot}$ ($1.1 \times 10^6 L_{\odot}$ after lensing correction).

Depending on the physical conditions of the gas, the CMB radiation field can significantly affect how well CO gas can be observed

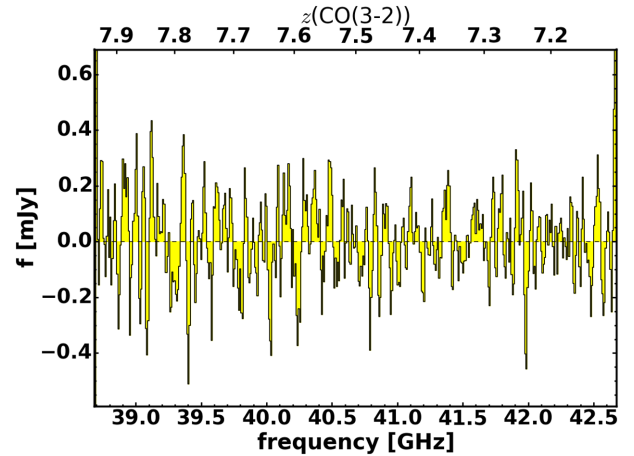


Figure 6. The observed GBT spectrum searching for CO(3-2) covering a redshift range of $z = 7.11-7.93$. For observed frequencies above 39.5 GHz, the 1σ rms is 0.14 mJy for the 8.79 MHz (~ 65 km s $^{-1}$ at 40.5 GHz) channels displayed here. The noise is slightly higher at the edge of the receiver band below 39.5 GHz. The CO(3-2) emission line was not detected.

at very high redshifts. According to the estimates from da Cunha et al. (2013) for $z \sim 7.5$, the observed flux of CO(3-2) could be about half of the intrinsic flux if the density and temperature are high ($T \sim 40$ K, $n_{\text{H}_2} \sim 10^{4.2}$ cm $^{-3}$), and this ratio would be lower for lower temperature and densities. Thus the effect of the CMB could explain why we do not detect the CO(3-2). We note that cosmic ray destruction of CO has been suggested as mechanism to remove CO from the molecular gas mass (e.g. Bisbas, Papadopoulos & Viti 2015).

Under the assumption that half of the intrinsic flux is missed due to the CMB radiation field and that the CO(3-2) is thermally excited, we estimate an upper limit on the molecular gas mass of $7.2 \times 10^9 M_{\odot}$ using a conversion factor $\alpha_{\text{CO}} = 4 M_{\odot} \text{ K km s}^{-1} \text{ pc}^2$ (e.g. Carilli & Walter 2013). Given the large number of assumptions, this should be viewed as an order of magnitude estimate. Using the size estimate from the ALMA continuum observations, assuming a simple geometry, this would imply an average gas density < 250 cm $^{-3}$.

4 DISCUSSION

A1689-zD1 is currently unusual among $z > 7$ galaxies in that it is detected in thermal dust emission and has a spectroscopically confirmed redshift without Ly α emission. The observations presented here also show that the galaxy is relatively small, with the galaxy resolved into two separate components, both in thermal dust emission and stellar continuum. Despite its relative modest size, the mean stellar surface density of about $1000 M_{\odot} \text{ pc}^{-2}$ is not exceptionally high, however, the SFR surface density of $\sim 7 M_{\odot} \text{ yr}^{-1} \text{ kpc}^{-2}$ as traced from the dust emission, is similar to that of starbursts (e.g. Bouché et al. 2007); we note that the SFR surface density could be partly overestimated if the size estimate from the sub-mm imaging has been underestimated because of the contrast against the CMB [this effect is discussed in Zhang et al. (2016)]. Given the very high redshift of the galaxy, questions naturally arise over how the galaxy came to be dusty and have apparently high metallicity this early, its lack of strong UV and FIR emission lines, and its morphology.

4.1 Could A1689-zD1 be a merging galaxy pair?

In order to assess the possibility of A1689-zD1 being a merging galaxy pair, we estimate the descendant halo mass using the

abundance matching technique, and use the results from N -body cosmological simulations to approximate the average merger rate. With a lensing-corrected UV luminosity of $\sim 1.8 \times 10^{10} L_{\odot}$, the mean halo mass of A1689-zD1 is $\sim 10^{11} M_{\odot}$ at $z = 7.5$ (with a virial radius ~ 11 kpc). Specifically, we use the relation by Schultz et al. (2014); see their fig. 6. This estimate is uncertain by a factor of ~ 2 , e.g. see fig. 15 of Harikane et al. (2016). The cumulative number of halo mergers with a mass ratio larger than ξ_{\min} , between redshifts z_0 and z that a descendant halo of mass $M_0(z_0)$ has suffered is,

$$N_m(\xi_{\min}, M_0, z_0, z) = \int_{z_0}^z dz \int_{\xi_{\min}}^1 d\xi \frac{dN_m}{d\xi dz}[\langle M(z) \rangle, \xi, z] \quad (1)$$

where $dN_m/d\xi/dz$ is the mean merger rate in units of mergers per halo per unit redshift per unit ξ , and $\langle M(z) \rangle$ is the mean halo mass assembly history. In order to compute equation (1), we take the results of Fakhouri, Ma & Boylan-Kolchin (2010) based on the statistics of the Millennium II simulation (specifically, their fitting formulae 1 and 2). Given the observed features of A1689-zD1, we assume a major merger with a mass ratio of at least $\xi_{\min} = 0.3$. If we further take $z_0 = 7.5$ and $z = 15$ (the maximum redshift where the formulae can be trusted) in equation (1), we find that $N_m \sim 2.1$. This number is most sensitive to the initial redshift z , e.g. it drops by a factor of ~ 4 if $z = 9$ instead of $z = 15$. Albeit given the evolved nature of the galaxy, it likely formed its first stars earlier than $z \sim 10$, thus N_m is likely larger than 0.5. We can then conclude that a merger under the conditions of A1689-zD1, should be a common occurrence according to our knowledge of structure formation. With such a mass ratio, and a descendant mass, a merger will occur in a time-scale (governed by dynamical friction) of $\mathcal{O}(100\text{Myr})$ [Binney & Tremaine 1987; calibrated with the results of Boylan-Kolchin et al. (2008)]. This time-scale is defined from the time the virial radii of the two haloes started to overlap.

The clumpy structure of A1689-zD1 could possibly also be the result of gravitational instabilities if A1689-zD1 is a disc galaxy in formation. Modelling by Ceverino, Dekel & Bournaud (2010) shows that giant clumps can arise in a scenario where cold streams providing the gas can cause discs to be gravitationally unstable and turbulent. Signatures of clumps in disc galaxies and ‘protodiscs’ are found both in optical studies of high- z spiral galaxies (e.g. Elmegreen et al. 2009a,b) and in molecular gas studies (e.g. Tacconi et al. 2010), where the latter finds clumps with masses $\sim 5 \times 10^9 M_{\odot}$ and intrinsic radii $< 1 - 2$ kpc. We do not have the observational results to constrain whether A1689-zD1 is a merging galaxy pair or the result of cold-mode accretion, however, the important point is that the structure we observe is similar in both the near-infrared (i.e. rest frame UV) and thermal dust emission, indicative of a dynamically perturbed system.

In either case of interacting galaxies or clumpy structure arising from dynamical instabilities, the average density of the gas is increased and the SFR will increase. A1689-zD1 has a comparatively high SFR and dust continuum emission, and with a stellar mass of $\sim 10^9 M_{\odot}$ it is expected that the metallicity is not low. These conditions seem to make A1689-zD1 suitable for accelerated grain growth, since undergoing a merger episode or dynamical instability could enhance the gas density and thus potentially provide the necessary conditions for grain growth in the ISM. For example, Mancini et al. (2015) present modelling where the time-scale for ISM grain growth is inversely proportional to the density of the gas and based on their model they suggest that the gas density of A1689-zD1 is very high, possibly comparable to quasar host galaxies (e.g. Valiante et al. 2014; Mancini et al. 2015). However, given

the uncertainties surrounding ISM grain growth (e.g. Ferrara, Viti & Ceccarelli 2016), we note that conditions in the galaxy certainly do not rule out direct SN dust production, and we await firmer limits on dust destruction by SN shocks to decide this question one way or the other.

4.2 Redshift

A1689-zD1 is one of the highest redshift galaxies known currently thanks to the spectroscopic redshift determination. The VLT X-Shooter spectrum covered a wide wavelength range, both in the optical and near-infrared. As presented in Watson et al. (2015), the redshift is determined from a clear break around $\sim 1 \mu\text{m}$, though no lines were detected, resulting in an accuracy of $\sigma_z \sim 0.2$. One of the goals of the ALMA and GBT observations was to observe line emission in order to get an accurate measurement of the redshift. As mentioned previously, both the ALMA and GBT data provide a wide coverage for two lines that in lower redshift star-forming galaxies would be bright. We obtain a tentative 3σ detection of the [C II] line with a corresponding redshift of $z_{[\text{C II}]} = 7.603$, however, deeper observations are necessary to confirm this. It is possible that the systemic redshift of A1689-zD1 may not have been covered by the observations. Adopting $\sigma_z \sim 0.2$ as a 68 per cent confidence interval, which is very conservative, this corresponds to a minimum 80 per cent coverage of the probability interval for the [C II] line, and similarly a minimum 95 coverage for the CO(3-2) line. We will work in the next section on the assumption that we cover these emission lines in these observations. Equally, however, non-detections of these two lines could also be due to astrophysical reasons in A1689-zD1 itself [see Sections 3.3 and 4.3, also see e.g. Maiolino et al. (2015) for an example of $z > 7$ galaxies with [C II] non-detections]. We explore this possibility below.

4.3 [C II]/ L_{FIR} deficit?

With the upper limit from the tentative detection of [C II] we find that the luminosity ratio is $L_{[\text{C II}]} / L_{\text{FIR}} < 0.0002$. This is low in comparison to local star-forming galaxies (e.g. Malhotra et al. 2001; Díaz-Santos et al. 2013), which typically have luminosity ratios of 0.0007–0.007 for galaxies with $L_{\text{FIR}} < 10^{11} L_{\odot}$. In fact the limit is closer to the ratios typically obtained for massive, luminous starbursts found in some quasar host galaxies (e.g. Wang et al. 2013), indicating that A1689-zD1 is [C II] deficient. While the reasons for this deficit observed towards several massive starbursts remain unclear, a number of possible explanations have been suggested (e.g. Luhman et al. 2003; Stacey et al. 2010). For example, a high-radiation field relative to the gas density could cause an increased far-infrared luminosity compared to several emission lines such as [C II] (e.g. Luhman et al. 2003; Abel et al. 2009). If the gas density exceeds the critical density of [C II], collisional de-excitation will become important and reduce the cooling by [C II] (e.g. Goldsmith et al. 2012). Alternatively, if the gas temperature exceeds the excitation temperature of the [C II] line, a saturation of the upper fine-structure level would occur, resulting in a maximum $L_{[\text{C II}]}$ even at increasing L_{FIR} (e.g. Muñoz & Oh 2016). A recent model from Narayanan & Krumholz (2016) suggests that the surface density plays an important role, i.e. an increase of the gas surface density would lower the total amount of C^+ and an increase of CO, which would result in a decreased $L_{[\text{C II}]} / L_{\text{FIR}}$ ratio.

In nearby star-forming galaxies, [C II] has been found to be reliable tracer of the SFR (e.g. De Looze et al. 2014; Díaz-Santos et al. 2014). It has thus been expected that [C II] would be a bright tracer of the star formation taking place even in the highest- z

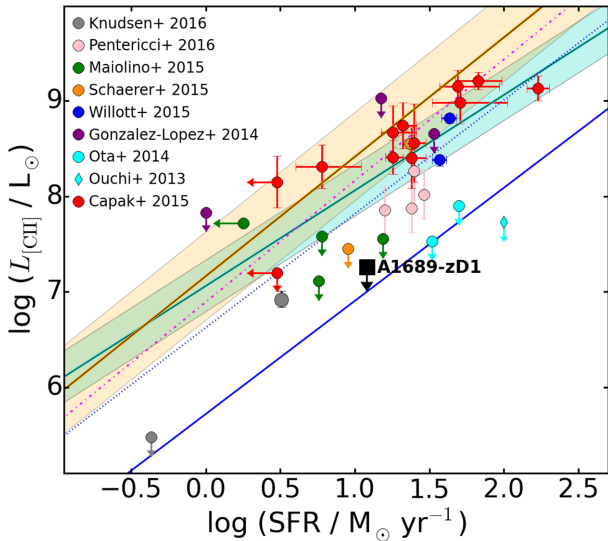


Figure 7. We plot the [C II] upper limit for A1689-zD1 after correcting for magnification (black square) against the star formation rate. We also include the recent $z \sim 6$ results from Ouchi et al. (2013), Ota et al. (2014), González-López et al. (2014), Willott et al. (2015b), Maiolino et al. (2015), Capak et al. (2015), Schaerer et al. (2015), Knudsen et al. (2016) and Pentericci et al. (2016). The $L_{[\text{C II}]}$ -SFR relations from De Looze et al. (2014) are shown for local star-forming galaxies (turquoise line and region) and for low-metallicity dwarf galaxies (orange line and region). The resulting relation from the low-metallicity simulations from Vallini et al. (2015) is indicated with the blue lines (solid: $Z = 0.05 Z_{\odot}$, dotted: $Z = 0.2 Z_{\odot}$) and the magenta dash-dotted line the results for massive $z \sim 2$ galaxies from Olsen et al. (2015).

galaxies, enabling discovery of sites of on-going (and obscured) star formation as well as enabling means to reliably measure SFRs. However, the non-detections of non-SMG and non-QSO star-forming galaxies have revealed a more complex picture of galaxy evolution during the first 0.5–1 Gyr after the big bang. In Fig. 7, we show the $L_{[\text{C II}]}$ -SFR relation for $z > 6$ star-forming galaxies including A1689-zD1 in comparison with the relations derived from low- z galaxies.

The lack of [C II] detections towards a large number of $z > 6$ star-forming galaxies has been discussed to be the consequence of low metallicity (González-López et al. 2014; Ota et al. 2014; Capak et al. 2015; Maiolino et al. 2015; Schaerer et al. 2015; Willott et al. 2015b; Knudsen et al. 2016). Low metallicity could bring down the expected [C II] line luminosity. In fact modelling of the gas in $z > 6$ galaxies suggests that the local SFR- $L_{[\text{C II}]}$ relation is decreased significantly depending on the metallicity (e.g. Vallini et al. 2015). However, an explanation involving low metallicity in A1689-zD1 is hard to reconcile with the high dust mass in this galaxy, a dust mass that suggests a metallicity close to the solar value (Watson et al. 2015). This makes the [C II] deficiency here perplexing, and instead seems to point to a powerful radiation field or high gas densities as the likely culprits in depressing [C II] emission. However, the measured SFR of $\sim 12 M_{\odot} \text{ yr}^{-1}$ is below the characteristic mean SFR for this galaxy of $\sim 25 M_{\odot} \text{ yr}^{-1}$ (as calculated from the stellar mass divided by the best-fitting age from the SED), and is not indicative of a galaxy at the peak of a massive starburst event. This suggests that a powerful radiation field is not the most obvious explanation for the [C II] deficiency. Our detection of a large dust mass clearly demonstrates that this galaxy must have a relatively high metallicity already.

5 CONCLUSIONS

In this paper, we present resolved observations of the dust continuum emission from A1689-zD1, which is presently the most distant known galaxy ($z = 7.5 \pm 0.2$) with a detection of emission from thermal dust. Our findings are as follows.

(i) The deep band-6 and band-7 continuum observations show that the redshifted far-infrared emission is extended over two components, each of which has a FWHM size of $\sim 0.45 \text{ kpc} \times 1.9 \text{ kpc}$ (after correcting for the gravitational lensing). We note that the combination of ALMA sub-arcsec observations with gravitational lensing provides an efficient approach to resolving the structure of the dust-emitting region. The gross far-infrared morphology is similar to the morphology of rest-frame UV light. This suggests that the galaxy is either two proto-galaxies interacting/merging or a clumpy proto-galactic disc.

(ii) Based on bands 6 and 7 ALMA photometry we derive a dust temperature $T \sim 35 - 45 \text{ K}$ ($\beta = 1.5 - 2$) after correcting for the CMB radiation field. This implies a far-infrared luminosity of $1.8 \times 10^{11} L_{\odot}$ (corrected for lensing magnification), in agreement with our previous results based on single-band photometry.

(iii) Based on deep ALMA band-6 spectroscopy with a 15 GHz coverage, the [C II] line is not detected. We present a tentative 3σ detection, which would imply a systemic redshift of 7.603. Using the derived line intensity and luminosity of the tentative line, we find that the line is underluminous relative to the far-infrared luminosity in comparison with local normal star-forming galaxies. Compared to the SFR, the upper limit is similar to the growing number of [C II] non-detections in $z > 6$ star-forming galaxies. While the non-detection can be explained astrophysically, we emphasize that the possibility for a different redshift remains until a confirmed line-detection has been obtained.

(iv) The CO(3-2) line is not detected in the GBT observations. Given the high temperature of the CMB radiation field at $z \sim 7.5$, it is difficult to determine an upper limit, however, we place an estimate on the limit of the molecular gas of $< 7 \times 10^9 M_{\odot}$ (assuming a Galactic $L'_{\text{CO-to-}M_{\text{H}_2}}$ conversion).

Previous models for grain growth show that the time-scale is inversely proportional to the gas density. It is possible that the reported structure, indicative of galaxy interaction or clumps, could be the signature of increased gas density and thus accelerated grain growth. More importantly, the question remains whether the relatively large dust mass is special for A1689-zD1 or if future, deeper observations of large samples of galaxies will reveal a larger population of dusty, normal galaxies at $z > 7$.

ACKNOWLEDGEMENTS

We thank the staff of the Nordic ALMA Regional Center node for their very helpful support and valuable discussions on the ALMA data. We acknowledge the anonymous referee for useful suggestions for the manuscript. KK acknowledges support from the Swedish Research Council (grant No.: 621-2011-5372) and the Knut and Alice Wallenberg Foundation. LC is supported by YDUN grant No. DFF-4090-00079. AG has been supported by the EU Marie Curie Integration Grant ‘SteMaGE’ No. PCIG12-GA-2012-326466. JR acknowledges support from the ERC starting grant CALENDs (336736). JZ is supported by the EU under a Marie Curie International Incoming Fellowship, contract PIFI-GA-2013-62772. This paper makes use of the following ALMA data: ADS/JAO.ALMA#2013.1.01064.S. ALMA is a partnership of ESO (representing its member states),

NSF (USA) and NINS (Japan), together with NRC (Canada) and NSC and ASIAA (Taiwan) and KASI (Republic of Korea), in cooperation with the Republic of Chile. The Joint ALMA Observatory is operated by ESO, AUI/NRAO, and NAOJ.

REFERENCES

- Abel N. P., Dudley C., Fischer J., Satyapal S., van Hoof P. A. M., 2009, *ApJ*, 701, 1147
- Bañados E., Decarli R., Walter F., Venemans B. P., Farina E. P., Fan X., 2015, *ApJ*, 805, L8
- Binney J., Tremaine S., 1987, *Galactic Dynamics*. Princeton Univ. Press, Princeton, NJ
- Bisbas T. G., Papadopoulos P. P., Viti S., 2015, *ApJ*, 803, 37
- Bouché N. et al., 2007, *ApJ*, 671, 303
- Boylan-Kolchin M., Ma C.-P., Quataert E., 2008, *MNRAS*, 383, 93
- Bradač M. et al., 2016, preprint ([arXiv:1610.02099](https://arxiv.org/abs/1610.02099))
- Bradley L. D. et al., 2008, *ApJ*, 678, 647
- Capak P. L. et al., 2015, *Nature*, 522, 455
- Carilli C. L., Walter F., 2013, *ARA&A*, 51, 105
- Ceverino D., Dekel A., Bournaud F., 2010, *MNRAS*, 404, 2151
- Cicone C. et al., 2015, *A&A*, 574, A14
- da Cunha E., Charlot S., Elbaz D., 2008, *MNRAS*, 388, 1595
- da Cunha E. et al., 2013, *ApJ*, 765, 9
- De Looze I. et al., 2014, *A&A*, 568, A62
- Díaz-Santos T. et al., 2013, *ApJ*, 774, 68
- Díaz-Santos T. et al., 2014, *ApJ*, 788, L17
- Elmegreen B. G., Elmegreen D. M., Fernandez M. X., Lemonias J. J., 2009a, *ApJ*, 692, 12
- Elmegreen D. M., Elmegreen B. G., Marcus M. T., Shahinyan K., Yau A., Petersen M., 2009b, *ApJ*, 701, 306
- Fakhouri O., Ma C.-P., Boylan-Kolchin M., 2010, *MNRAS*, 406, 2267
- Ferrara A., Viti S., Ceccarelli C., 2016, *MNRAS*, 463, L112
- Finkelstein S. L. et al., 2013, *Nature*, 502, 524
- Goldsmith P. F., Langer W. D., Pineda J. L., Velusamy T., 2012, *ApJS*, 203, 13
- González-López J. et al., 2014, *ApJ*, 784, 99
- Harikane Y. et al., 2016, *ApJ*, 821, 123
- Iglesias-Páramo J. et al., 2007, *ApJ*, 670, 279
- Jullo E., Kneib J.-P., 2009, *MNRAS*, 395, 1319
- Jullo E., Kneib J.-P., Limousin M., Elíasdóttir Á., Marshall P. J., Verdugo T., 2007, *New J. Phys.*, 9, 447
- Kanekar N., Wagg J., Ram Chary R., Carilli C. L., 2013, *ApJ*, 771, L20
- Knudsen K. K., Richard J., Kneib J.-P., Jauzac M., Clément B., Drouart G., Egami E., Lindroos L., 2016, *MNRAS*, 462, L6
- Limousin M. et al., 2007, *ApJ*, 668, 643
- Luhman M. L., Satyapal S., Fischer J., Wolfire M. G., Sturm E., Dudley C. C., Lutz D., Genzel R., 2003, *ApJ*, 594, 758
- Maiolino R. et al., 2005, *A&A*, 440, L51
- Maiolino R. et al., 2015, *MNRAS*, 452, 54
- Malhotra S. et al., 2001, *ApJ*, 561, 766
- Mancini M., Schneider R., Graziani L., Valiante R., Dayal P., Maio U., Ciardi B., Hunt L. K., 2015, *MNRAS*, 451, L70
- Marti-Vidal I., Vlemmings W. H. T., Muller S., Casey S., 2014, *A&A*, 563, A136
- McMullin J. P., Waters B., Schiebel D., Young W., Golap K., 2007, in Shaw R. A., Hill F., Bell D. J., eds, *ASP Conf. Ser. Vol. 376, Astronomical Data Analysis Software and Systems XVI*. Astron. Soc. Pac., San Francisco, p. 127
- Michałowski M. J., 2015, *A&A*, 577, A80
- Michałowski M., Hjorth J., Watson D., 2010, *A&A*, 514, A67
- Muñoz J. A., Oh S. P., 2015, *MNRAS*, 463, 2085
- Narayanan D., Krumholz M., 2016, preprint ([arXiv:1601.05803](https://arxiv.org/abs/1601.05803))
- Oesch P. A. et al., 2015, *ApJ*, 804, L30
- Oesch P. A. et al., 2016, *ApJ*, 819, 129
- Olsen K. P., Greve T. R., Narayanan D., Thompson R., Toft S., Brinch C., 2015, *ApJ*, 814, 76
- Ono Y. et al., 2012, *ApJ*, 744, 83
- Ota K. et al., 2014, *ApJ*, 792, 34
- Ouchi M. et al., 2013, *ApJ*, 778, 102
- Pentericci L. et al., 2016, *ApJ*, 829, L11
- Planck Collaboration XVI, 2014, *A&A*, 571, A16
- Riechers D. A. et al., 2013, *Nature*, 496, 329
- Schaerer D., Boone F., Zamojski M., Staguhn J., Dessauges-Zavadsky M., Finkelstein S., Combes F., 2015, *A&A*, 574, A19
- Schenker M. A., Stark D. P., Ellis R. S., Robertson B. E., Dunlop J. S., McLure R. J., Kneib J.-P., Richard J., 2012, *ApJ*, 744, 179
- Schultz C., Oñorbe J., Abazajian K. N., Bullock J. S., 2014, *MNRAS*, 442, 1597
- Shibuya T., Kashikawa N., Ota K., Iye M., Ouchi M., Furusawa H., Shimasaku K., Hattori T., 2012, *ApJ*, 752, 114
- Silva L., Granato G. L., Bressan A., Danese L., 1998, *ApJ*, 509, 103
- Solomon P. M., Vanden Bout P. A., 2005, *ARA&A*, 43, 677
- Song M., Finkelstein S. L., Livermore R. C., Capak P. L., Dickinson M., Fontana A., 2016, *ApJ*, 826, 113
- Stacey G. J., Hailey-Dunsheath S., Ferkinhoff C., Nikola T., Parshley S. C., Benford D. J., Staguhn J. G., Fiolet N., 2010, *ApJ*, 724, 957
- Tacconi L. J. et al., 2010, *Nature*, 463, 781
- Valiante R., Schneider R., Salvadori S., Gallerani S., 2014, *MNRAS*, 444, 2442
- Vallini L., Gallerani S., Ferrara A., Pallottini A., Yue B., 2015, *ApJ*, 813, 36
- Vanzella E. et al., 2011, *ApJ*, 730, L35
- Venemans B. P. et al., 2012, *ApJ*, 751, L25
- Venemans B. P., Walter F., Zschaechner L., Decarli R., De Rosa G., Findlay J. R., McMahon R. G., Sutherland W. J., 2016, *ApJ*, 816, 37
- Wang R. et al., 2013, *ApJ*, 773, 44
- Watson D., Christensen L., Knudsen K. K., Richard J., Gallazzi A., Michałowski M. J., 2015, *Nature*, 519, 327
- Willott C. J., Bergeron J., Omont A., 2015a, *ApJ*, 801, 123
- Willott C. J., Carilli C. L., Wagg J., Wang R., 2015b, *ApJ*, 807, 180
- Zhang Z.-Y., Papadopoulos P. P., Ivison R. J., Galametz M., Smith M. W. L., Xilouris E. M., 2016, *R. Soc. Open Sci.*, 3, 160025
- Zitrin A. et al., 2015, *ApJ*, 810, L12

APPENDIX A: MAPPING OF CANDIDATE EMISSION LINES

As described in Section. 3.2, in order to search for the [C II] line in the ALMA band-6 data, we imaged all the positive spectral features with flux >0.6 mJy, which corresponds to $\sim 2\sigma$ in the Hanning-smoothed spectrum. In this Appendix, we show the maps constructed using a width of 0.1 GHz. In Fig. A1, we show the maps as contours overlaid on the near-infrared F160W *HST* image. A couple of the features show image contours of $\sim 2.5\sigma$ around the position of A1689-zD1. The features of 220.903, 223.770, and 228.000 GHz show 3σ contours, however, only in the case of 220.903 GHz are they following the same position as the dust continuum. We note that this is possibly the best-candidate line for redshifted [C II] and therefore report it as a tentative detection.

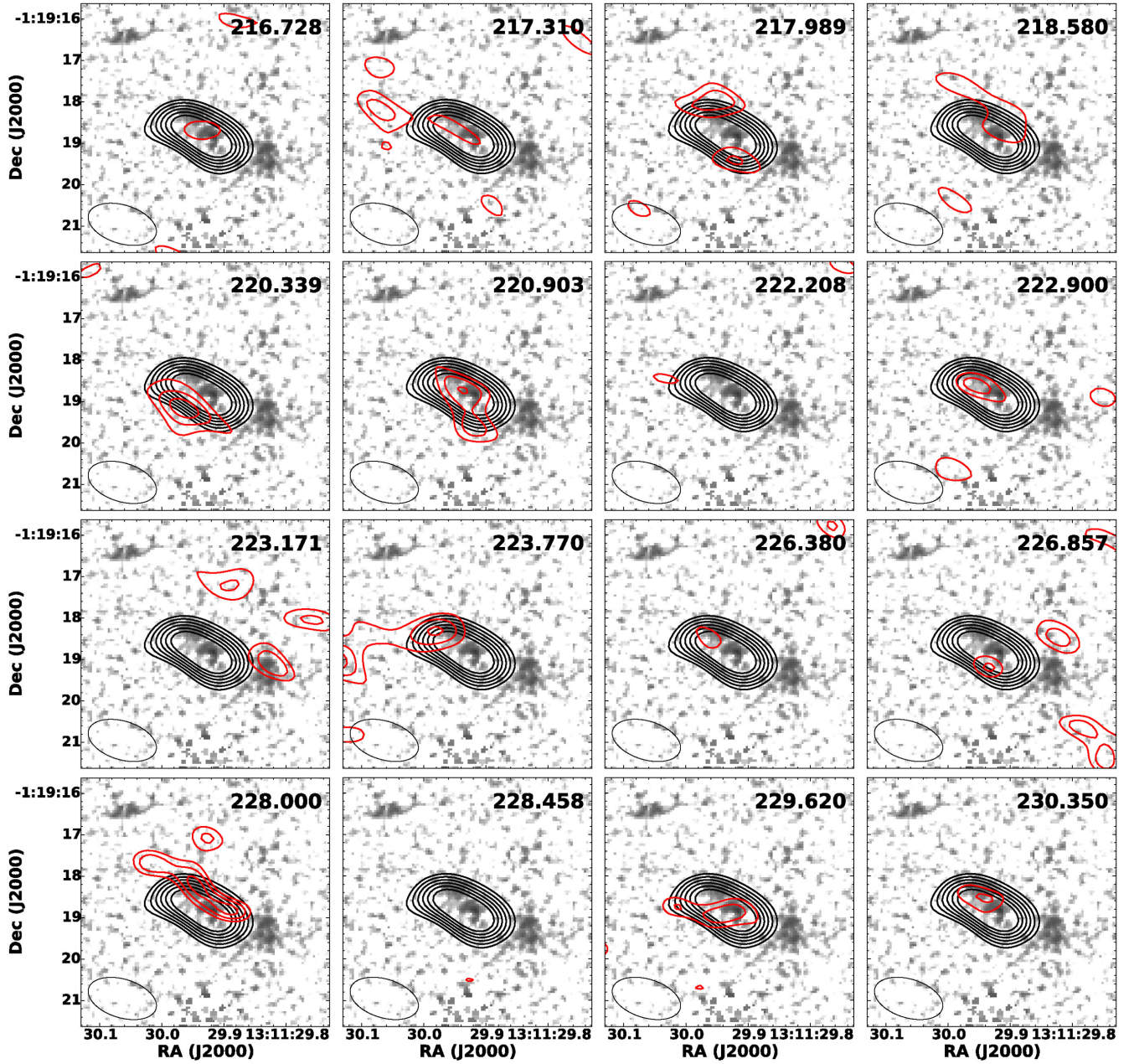


Figure A1. Images from integrating over 0.1 GHz at different frequencies. Red contours correspond to 2σ , 2.5σ , and 3σ , where σ is the rms measured in each image. The frequency is written in the upper-left corner of each sub-image and indicated with a green arrow on top of the spectrum shown in Fig. 4. As in Fig. 5, the black contours show the continuum image with natural weighting (5σ , 6σ , 7σ , 8σ , 9σ , and 10σ); the grey-scale image is the same as in Figs 1 and 5.

This paper has been typeset from a $\text{\TeX}/\text{\LaTeX}$ file prepared by the author.